

# Thermal and Dynamical Evolution of Primordial Gas Clouds

— On the Formation of First Luminous Objects —

Ryoichi NISHI,<sup>\*)</sup> Hajime SUSA,<sup>\*,\*\*)</sup> Hideya UEHARA,<sup>\*\*,\*\*\*)</sup>  
 Masako YAMADA,<sup>\*\*\*\*)</sup> and Kazuyuki OMIKAI<sup>\*\*\*\*\*)</sup>

*Department of Physics, Kyoto University, Kyoto 606-8502, Japan*

*\* Center for Computational Physics, University of Tsukuba  
 Tsukuba 305-8571, Japan*

*\*\* Division of Theoretical Astrophysics, National Astronomical Observatory  
 Mitaka 181-8588, Japan*

(Received September 21, 1998 )

We investigate the thermal and dynamical evolution of primordial gas clouds in the universe after decoupling. Comparing the time-scale of dynamical evolution with that of fragmentation, we can estimate the typical fragmentation scale. We propose the following scenario of the formation process of first luminous objects consisting of large number stars. First, by pancake collapse of the overdensity regions in the expanding universe or collision between clouds in potential wells, quasi-plane shocks form. If the shock-heated temperature is higher than about  $10^4$  K, the postshock gas cools down to several hundred K by H<sub>2</sub> line cooling, and the shock-compressed layer fragments into filamentary clouds. The filamentary cloud collapses dynamically once more and fragments into cloud cores. Finally, a primordial star forms in a cloud core. We show that the minimum mass of the first star is essentially determined by the *Chandrasekhar mass*. Also, we investigate the dynamical collapse of cloud cores by numerical simulation and show that the evolution paths of the central regions of the cores depend only very weakly on the total core mass. After mass accretion, a massive star may be formed in a core, since the estimated mass accretion rate is very large. In such a case, it may be possible for many massive stars form almost simultaneously. Then the clouds can be luminous objects. On the other hand, if the shock-heated temperature is lower, effective star formation is delayed significantly.

## §1. Introduction

Today, we have a great deal of observational data concerning the early universe. However, we have very little information about an era referred to as the ‘dark ages’. Information regarding an era of recombination (with redshift  $z$  of about  $10^3$ ) can be obtained by observation of cosmic microwave background radiation. After recombination we can obtain little information until  $z \sim 5$ , when we can observe luminous objects such as galaxies and QSOs. On the other hand, formation stage of these objects should be in the ‘dark ages’, and thus investigating the formation process of galaxies using a theoretical approach is very important.

---

<sup>\*)</sup> E-mail: nishi@tap.scphys.kyoto-u.ac.jp

<sup>\*\*)</sup> E-mail: susa@rccp.tsukuba.ac.jp

<sup>\*\*\*)</sup> E-mail: uehara@th.nao.ac.jp

<sup>\*\*\*\*)</sup> E-mail: masako@tap.scphys.kyoto-u.ac.jp

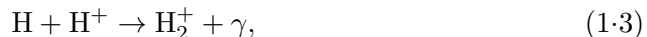
<sup>\*\*\*\*\*)</sup> E-mail: omukai@tap.scphys.kyoto-u.ac.jp

In the standard theory of the formation of luminous objects, the most basic idea is that they are made from giant gas clouds, which were once slightly overdense regions in the early epoch and grew to depart from the general cosmic expansion. After contraction of these clouds, if they fragment into many stellar-size clouds and many massive stars are formed on a time scale of the life of the massive stars ( $10^7$  yr), they can become luminous objects. To understand the way in which luminous objects are formed, we investigate physical processes of the clouds in various stages of evolution.

To discuss the formation and evolution of galaxies, it is necessary to investigate star formation processes in protogalactic clouds, since stars are very important components of observed galaxies. In addition, stars play crucial roles in galactic activities, for example, ultraviolet radiation and supernova explosions, which are important in some cosmological contexts. Moreover, considering the hierarchical clustering scenario, several authors have stressed the importance of stars in pregalactic objects for the reionization of the universe (e.g., Ref. 1)). Therefore, to study galaxy formation and evolution of intergalactic matter, it is necessary to investigate the star formation process in the early universe.

Because gravity alone cannot be used to derive natural scales, to form objects of various scales, such as galaxies and stars, thermal processes within gases are very important. In the early epoch, before the first stars were formed, baryonic matter was made mostly of hydrogen and helium, and the most important coolants at relatively low temperature was hydrogen molecules. Without hydrogen molecules, gas clouds of primordial composition are ineffective to cool below about  $10^4$  K, because of the high energy of hydrogen Ly $\alpha$  photons. Hence the Jeans mass of a purely atomic gas of primordial composition is about  $M_J \propto T^{3/2} \rho^{-1/2} \sim 10^7 (T/10^4 \text{ K})^{3/2} (n/1 \text{ cm}^{-3})^{-1/2} M_\odot$ , far larger than the stellar scale. Sufficiently after the recombination ( $z_{\text{rec}} \sim 1100$ ), the fraction of H<sub>2</sub> is frozen at a constant value of order  $10^{-5}$ ,<sup>2)</sup> and this small amount of H<sub>2</sub> is not enough to cool the gas in order to lower the Jeans mass down to stellar mass within the age of the universe. Hence the length scale into which the clouds fragment depends strongly on the amount of H<sub>2</sub> which is formed in the clouds during their contraction.

Because of the absence of dust grains and the inefficiency of direct reaction (H + H  $\rightarrow$  H<sub>2</sub> +  $\gamma$ ), H<sub>2</sub> molecules are formed through the two indirect paths described below:



Both paths require a certain degree of ionization, and usually the first path is more effective than second path. Hydrogen molecules are collisionally dissociated efficiently at  $T \gtrsim$  several thousand K. Then, in order for H<sub>2</sub> to be made through the

above two reactions, there must be some degree of ionization at  $T \lesssim 10^4$  K. On the other hand, if in chemical equilibrium, there remain few electrons or  $\text{H}^+$  ions at  $T \lesssim 10^4$  K. In such clouds, little  $\text{H}_2$  can be formed. When  $z \gtrsim 10^2$ ,  $\text{H}^-$  is radiatively detached by cosmic background radiation and  $\text{H}_2$  formation is inefficient.<sup>2), 3)</sup> Thus, we consider clouds collapsing only when  $z \lesssim 10^2$ .

In addition, the thermal evolution of clouds is strongly affected by the initial shape of the clouds, or their angular momentum in the initial state.<sup>4)</sup> The collapse of an initially oblate cloud is very different from that of spherical one. The non-spherical collapse in the initial phase is immediately followed by a disk-like collapse, which has a different time scale from a spherical collapse. Strictly speaking, the times needed for  $\rho$  to be  $\infty$  do not differ greatly from each other, but *at the same density*, which is much higher than the initial value, the time scales determined by the temporal shrinking rates are entirely different. For spherical collapse we have

$$t_{\text{dyn}} \equiv -r/v_r \propto \rho^{-1/2} \text{ (free fall time),} \quad (1.5)$$

and for disk-like collapse,

$$t_{\text{dyn}} \equiv -z/v_z \propto \rho^{-1} \text{ (} z \rightarrow 0\text{).} \quad (1.6)$$

Since, after sufficient collapse,  $v_z$  is almost constant and  $z$  changes as  $\rho^{-1}$ . Then  $t_{\text{dyn}}$  for disk-like collapse becomes much shorter than the free-fall time at the same density. And this time scale  $t_{\text{dyn}}$  is also the time scale of adiabatic heating. So the thermal evolution of these oblate spheroids is also very different from that of spherical clouds. Moreover, thin disk-like clouds can fragment into smaller clouds. Then it is necessary to include the effect of shape change when we investigate the thermal evolution and the fragmentation of clouds.

In this paper, we put together important physical processes regarding cloud evolution in the early universe in various evolutionary stages. In §2 we investigate the thermal and dynamical evolution of primordial gas clouds and discuss fragmentation processes. In §3 we discuss cylindrical collapse, which follows fragmentation of the disk-like cloud. In §4 we investigate the evolution of cloud cores and discuss the formation of stellar cores. Finally, we summarize our results and discuss the formation of first luminous objects in §5.

## §2. Contraction and fragmentation processes of primordial gas clouds

In this section, we investigate the processes of contraction and fragmentation of primordial gas clouds. To discuss cloud evolution, we compare various time scales. And we consider that a collapsing cloud fragments when the condition

$$t_{\text{dyn}} \sim t_{\text{frag}}, \quad (2.1)$$

is satisfied, where

$$t_{\text{dyn}} \left( \equiv \rho / \frac{d\rho}{dt} \right) : \text{the timescale for dynamical evolution,}$$

$$t_{\text{frag}} : \text{the timescale for fragmentation.}$$

### 2.1. Initial pressure-free collapse

First, a cloud with a mass much larger than its own virial mass collapses almost as a free-fall collapse. Several authors investigated the thermal evolution of primordial clouds in pressure-free collapse with a 1-zone approximation.<sup>3), 5), 6)</sup> They also estimated the minimum Jeans mass of a collapsing cloud.

However, spherical clouds in pressure-free collapse are unstable against non-spherical perturbations<sup>7)</sup> and eventually they collapse into a disk-like configuration.<sup>4)</sup> The effective ‘adiabatic index’,  $\Gamma \equiv \frac{\partial \ln p / \partial t}{\partial \ln \rho / \partial t}$ , changes with the collapse configuration, and, moreover, the critical  $\Gamma$ , which corresponds to occurrence of bounce, also changes: it is 0 for disk collapse, 1 for cylindrical collapse, and 3/4 for spherical collapse. Thus we investigated the thermal evolution of non-spherical primordial gas clouds.<sup>8)</sup> We studied the influence of the angular momentum and/or initial shape of the clouds in pressure-free collapse using a calculation of thermal evolution including radiative transfer. We show that ordinary clouds bounce and are shock-heated when the hydrogen number density is much lower than  $10^8 \text{ cm}^{-3}$ , which is the density at which three-body reaction for  $\text{H}_2$  formation becomes important. Therefore the Jeans mass cannot be lowered to the stellar mass scale in this stage.

### 2.2. Evolution of post shock gas

As discussed above, ordinary pregalactic clouds collapse into disk-like configurations and are shock-heated when they bounce. Also, when subgalactic clouds collide, they are shock-heated. After considerable cooling, a shock-compressed layer can fragment into smaller clouds. Thus, we study the thermal evolution of the post-shock flow.<sup>9)</sup>

#### 2.2.1. Important time scales

First, we compare the time scales which are essential to the thermal evolution of the postshock layer in primordial gas clouds. The various relevant time scales are

$$t_{\text{cool}} \equiv C_p \frac{\rho k T}{\mu m_p \Lambda}, \quad (2.2)$$

$$t_{\text{ion}} \equiv \frac{n_p}{k^{\text{ion}} n_{\text{H}} n_e} = \frac{1}{k^{\text{ion}} n_N (1 - y_e)}, \quad (2.3)$$

$$t_{\text{rec}} \equiv \frac{n_p}{k^{\text{rec}} n_e n_p} = \frac{1}{k^{\text{rec}} n_N y_e}, \quad (2.4)$$

$$t_{\text{dis}} \equiv \frac{n_{\text{H}_2}}{\dot{n}_{\text{H}_2}^{\text{dis}}}, \quad (2.5)$$

$$t_{\text{for}} \equiv \frac{n_{\text{H}_2}}{\dot{n}_{\text{H}_2}^{\text{for}}}, \quad (2.6)$$

where  $t_{\text{cool}}$ ,  $t_{\text{ion}}$ ,  $t_{\text{rec}}$ ,  $t_{\text{dis}}$  and  $t_{\text{for}}$  denote the time scales of cooling, ionization, recombination,  $\text{H}_2$  dissociation and formation, respectively. \*)  $n_N$ ,  $n_i$ ,  $y_i$  ( $\equiv n_i/n_N$ ),  $k^X$ ,  $\rho$ ,  $\mu$

---

\*) The time scale of thermalization in the post-shock layer is shorter than the other time scales. For example, at  $2 \times 10^4 \text{ K}$  the time scales of thermalization for plasma and neutral gas are about  $10^2$  and  $10^5$  times shorter than the ionization time scale, respectively.

and  $m_p$  are the number density of nucleons, the number density of the  $i$ th species, the fraction of  $i$ th species, the chemical reaction rate coefficient of the “X” process, the mass density, mean molecular weight and proton mass, respectively.  $\Lambda$  denotes the net cooling rate, which includes radiative and chemical cooling/heating. We assume that the system is optically thin for cooling photons. This assumption is valid for usual subgalactic clouds. For simplicity, we do not include helium. The existence of helium affects the mean molecular weight and the cooling rate at high temperature ( $T \sim 10^5$  K). However, these are minor effects on the thermal evolution of primordial gas clouds at lower temperature ( $T \lesssim 10^4$  K), which we are especially interested in.  $C_p$  denotes the heat capacity of the gas cloud. Since we are interested in a quasi-steady post-shock flow, where  $t_{\text{cool}}$  is shorter than the time scale of the change of the shock velocity and/or pre-shock density, the post-shock layer is almost isobaric.  $\dot{n}_{\text{H}_2}^{\text{dis}}$  and  $\dot{n}_{\text{H}_2}^{\text{for}}$  denote the effective  $\text{H}_2$  dissociation and formation rate. Since  $\text{H}_2$  molecules are formed through  $\text{H}^-$  or  $\text{H}_2^+$  (Eqs. (1.1) to (1.4)) and dissociated through  $\text{H}_2^+$ ,<sup>2)</sup> we include only the part of reaction rate, that corresponds to the reaction formed from H and dissociated to H. Comparing these five time scales we can find the fastest process without solving detailed time-dependent differential equations.

We should remark that *all of these time scales are proportional to  $\rho^{-1}$*  if the cooling rate and all reaction rates are proportional to  $\rho^2$ . The dominant component of the cooling changes according to temperature. Below  $10^4$  K,  $\text{H}_2$  line emission dominates the total cooling of the cloud. In this process, the cooling rate is proportional to the number density of the hydrogen molecules at the excited levels whose fraction is proportional to  $\rho$ .<sup>\*)</sup> Hence, the cooling time scale is proportional to  $\rho^{-1}$  for  $T \lesssim 10^4$  K, as in equation (2.2). The cooling process in the temperature range  $10^4 \text{ K} \lesssim T \lesssim 10^5 \text{ K}$  is dominated by the bound-bound transition of the hydrogen atoms, and the number of excited hydrogen atoms is determined by collisions with other atoms. Therefore, the cooling rate is proportional to the square of the total density. For higher temperatures ( $T \gtrsim 10^5$  K), the free-free emission by the collision between ions and electrons dominates the energy radiated away from the cloud. In any case, the cooling rate is proportional to  $\rho^2$ , and the cooling time is proportional to  $\rho^{-1}$ .<sup>\*\*)</sup> The chemical reaction rates are proportional to  $\rho^2$  if the reactions are dominated by collisional processes.

Photoionization and  $\text{H}_2$  photodissociation processes caused by the UV photons emitted from the post-shock hot region could affect the ionization rates and the  $\text{H}_2$  dissociation rates in post-shock regions. These radiative reactions are proportional to  $\rho^2$ , because the emission rate of UV photons in the post-shock is proportional to  $\rho^2$ . We investigate the effects of UV photons from postshock regions.<sup>14)</sup> However, as a 0th-order approximation, we neglect the photoionization and the  $\text{H}_2$  photodissociation processes in this paper.

---

\*) This treatment is limited to low density ( $n \lesssim 10^4 \text{ cm}^{-3}$ ) The cooling rate is not proportional to  $\rho^2$  for higher density (higher than the *critical density*).

\*\*\*) Compton cooling is effective at high redshift and high temperature. In this case, the cooling rate is not proportional to  $\rho^2$ , but this does not change the following results significantly.

### 2.2.2. Fraction of H<sub>2</sub>

Here we consider the estimation of  $y_{\text{H}_2}$  in the post-shock flow for the case in which the post-shock temperature is higher than about  $10^4$  K. If  $y_{\text{H}_2}$  can be determined for given  $T$  and  $y_e$ , the cooling time is always determined by just  $T$  and  $y_e$ . As a result, the thermal evolution of the system is completely determined in the  $y_e$ - $T$  plane.

Now, we make some remarks regarding important properties of  $t_{\text{dis}}$  and  $t_{\text{for}}$ . First, the time scale of dissociation is independent of  $y_{\text{H}_2}$ , the fraction of hydrogen molecules. On the other hand,  $t_{\text{for}}$  is proportional to  $y_{\text{H}_2}$ . Then, the time scales given in terms of their equilibrium values are

$$t_{\text{dis}} = t_{\text{dis}}^{\text{eq}}, \quad (2.7)$$

$$t_{\text{for}} = t_{\text{for}}^{\text{eq}} \frac{y_{\text{H}_2}}{y_{\text{H}_2}^{\text{eq}}(y_e, T)} = t_{\text{dis}}^{\text{eq}} \frac{y_{\text{H}_2}}{y_{\text{H}_2}^{\text{eq}}(y_e, T)}, \quad (2.8)$$

where the suffix eq denotes the value at which the hydrogen molecules are in chemical equilibrium for a given electron abundance and temperature. Thus,  $t_{\text{dis}} < t_{\text{rec}}$ ,  $t_{\text{cool}}$  is a sufficient condition  $y_{\text{H}_2}$  to be the equilibrium value for given  $y_e$  and  $T$ .

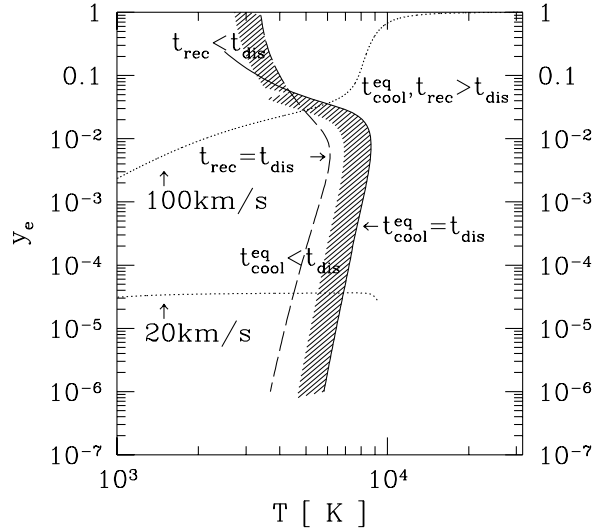


Fig. 1. The  $y_e$ - $T$  plane is divided into two regions, one in which chemical equilibrium is achieved for a fraction of hydrogen molecules and one in which this is not the case. The solid boundary of the shaded region is determined by the condition  $t_{\text{cool}} = t_{\text{dis}}$ . The long dashed line denotes the boundary at which  $t_{\text{rec}} = t_{\text{dis}}$  is satisfied. In the shaded region, the chemical equilibrium of hydrogen molecules breaks down, and the fraction  $y_{\text{H}_2}$  freezes as the temperature and/or ionization degree drops. The dotted lines labeled ‘100 km/s’ and ‘20 km/s’ denote the evolutionary path of  $y_e$ .

We compare  $t_{\text{dis}}$  with  $t_{\text{rec}}$  and  $t_{\text{cool}}$  in the  $y_e$ - $T$  plane (Fig. 1). \*) At higher temperature,  $t_{\text{dis}}$  is shorter than  $t_{\text{rec}}$  and  $t_{\text{cool}}$ , and then  $y_{\text{H}_2} = y_{\text{H}_2}^{\text{eq}}(y_e, T)$ . After

\*) Note that Fig. 1 is corresponds to Fig. 2 of Susa et al.,<sup>9)</sup> but calculated using new reaction

cooling, in the shaded region, the chemical equilibrium of hydrogen molecules breaks down, and  $y_{\text{H}_2}$  almost freezes as the temperature and/or ionization degree drops. Thus, we can roughly determine  $y_{\text{H}_2}$  for given  $y_e$  and  $T$  in the cooling layers of post-shock flow.

### 2.2.3. Ionization and cooling

Here we investigate the case  $t_{\text{ion}} < t_{\text{rec}}$ , which corresponds to higher temperature ( $T \gtrsim 10^4$  K), and compare the time scale of ionization with that of cooling. The line along which  $t_{\text{ion}}/t_{\text{cool}}$  is equal to unity is indicated by the solid line in Fig. 2. If the initial conditions are given below the line, the system is ionized before it cools down, because  $t_{\text{ion}}/t_{\text{cool}} < 1$ . Otherwise, the system cools before it is ionized. The expected evolutionary path is also expressed by the arrows in Fig. 2.

### 2.2.4. Recombination and cooling

Next we investigate the case  $t_{\text{rec}} < t_{\text{ion}}$ , which corresponds to lower temperature and examine the balance between the recombination process and the cooling process. The recombination process is important for  $T \lesssim 10^4$  K. At  $T \lesssim 10^4$  K, the line cooling of the hydrogen molecules dominates the atomic hydrogen line cooling. Therefore the ratio  $t_{\text{rec}}/t_{\text{cool}}$  depends not only on the ionization degree and the temperature but also on the fraction of hydrogen molecules. In order to draw the line  $t_{\text{rec}}/t_{\text{cool}} = 1$  in the  $y_e$ - $T$  plane, we need information on the fraction of hydrogen molecules. The fraction of  $\text{H}_2$  is determined by the chemical equilibrium above  $\sim 10^4$  K. Then, it is approximately frozen below  $\sim 6 \times 10^3$  K through an evolutionary course with cooling. The line along which  $t_{\text{rec}}/t_{\text{cool}} = 1$  is satisfied is drawn in Fig. 2. In the region above the line, the system recombines before it cools down, and below the line, the system cools down before the recombination proceeds. The expected evolutionary path is also indicated in Fig. 2 by the arrows.

### 2.2.5. Shock diagram

The ratio of any two time scales is independent of the total density, and they are determined by the temperature and the chemical compositions ( $y_e$  and  $y_{\text{H}_2}$ ).  $y_{\text{H}_2}$  is almost always determined by  $y_e$  and  $T$ . Therefore, the ratio of any two time scales just depends on  $T$  and  $y_e$ . In the following sections, we compare the time scales individually.

The main results are summarized in Fig. 2. The evolution of a shock heated system is basically explained in the  $y_e$ - $T$  plane, which we call ‘‘shock diagram’’. The evolutionary path of the post-shock layer is obtained by tracing the directions of the arrows on the shock diagram. Post-shock gas, which is heated up to high temperature, appears in region (a). In region (a), the shortest time scale is  $t_{\text{ion}}$ , and the system evolves upward and enters region (b). In region (b),  $t_{\text{cool}}$  is the shortest, and therefore the system evolves leftward here and comes into region (c). In region (c),  $t_{\text{rec}}$  is the shortest. Then the system evolves downward and reenters the region (b), where it evolves leftward again and crosses the boundary of regions

---

rates and cooling function.<sup>2)</sup> There exist some quantitative differences, however. In particular, the line  $t_{\text{rec}} = t_{\text{dis}}$  changes somewhat. This is mainly because the dissociative recombination rate of  $\text{H}_2^+$  ( $\text{H}_2^+ + e \rightarrow 2\text{H}$ ) is reduced,<sup>2)</sup> and hence the effective  $\text{H}_2$  dissociation rate is reduced.

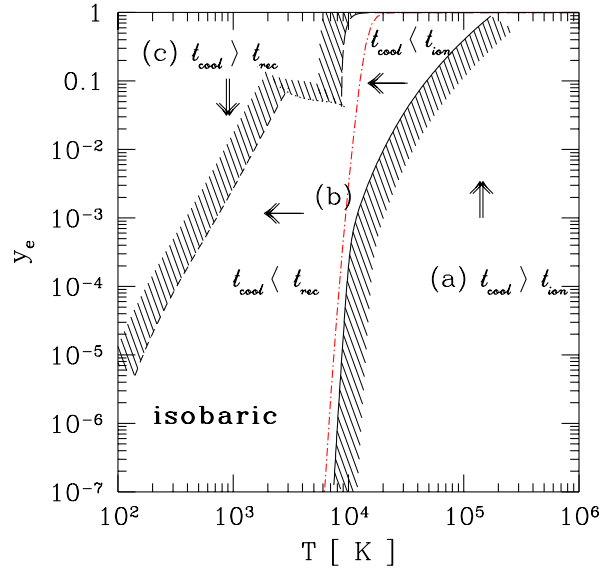


Fig. 2. The  $y_e$ - $T$  plane is divided into several regions in which the ratio of the time scales are different from each other. The arrows on the plane denote the directions of the evolution of the post-shock layer. The dot-short dashed line denotes the curve on which the equality  $t_{\text{rec}} = t_{\text{ion}}$  holds. The region (a) in which the condition  $t_{\text{ion}} < t_{\text{cool}}$  holds is bounded by the solid line. In this region, the system evolves upward in the  $y_e$ - $T$  diagram. In the region (b), the conditions  $t_{\text{cool}} < t_{\text{ion}}$ ,  $t_{\text{rec}}$  always holds. Therefore the temperature drops down before the system is further ionized or recombines. In the region (c) we have  $t_{\text{rec}} < t_{\text{cool}}$ , and the system evolves downward. The region (c) is bounded by the dotted line, short dashed line and the long dashed line. These three lines denote the boundary on which the condition  $t_{\text{cool}} = t_{\text{rec}}$  holds. The long dashed line is calculated by assuming that the cooling rate is dominated by hydrogen line cooling. The dotted line is calculated assuming the chemical equilibrium of the hydrogen molecules, and the short dashed line is calculated with  $y_{\text{H}_2} = 10^{-3}$ , which corresponds to the frozen value of the hydrogen molecules for a shock velocity higher than  $\sim 40$  km/s.

(b) and (c). Finally, the system evolves nearly along the short dashed curve which is the boundary of regions (b) and (c). For post-shock gas which is not heated above  $2 \times 10^4$  K, the thermal evolution is somewhat different from the previous case. In this case, when the system enters region (b) from region (a), the ionization degree is so low that the system does not enter region (c) at  $T \simeq 10^4$  K. Then the ionization degree and the fraction of hydrogen molecules do not “forget” the initial conditions of the chemical composition.

#### 2.2.6. Convergence of $y_e$ and $y_{\text{H}_2}$ in almost steady postshock flow

It is known that in steady post shock flow, both  $y_e$  and  $y_{\text{H}_2}$  become the same value at the same temperature. This is surprising because ionization equilibrium is not yet achieved at all. Now, the reason that convergence of  $y_e$  and  $y_{\text{H}_2}$  in the steady post-shock flow occurs can be understood using Figs. 1 and 2.

At  $T \sim 10^4$  K, the line  $t_{\text{rec}} = t_{\text{cool}}$  becomes nearly vertical, since the dominant cooling process is the hydrogen atomic line cooling, which decreases by many orders



below  $T \sim 3 \times 10^4$  K. If (1) the initial shock velocity is larger than  $\sim 40$  km/s or (2) the initial ionization degree is larger than  $\sim 5 \times 10^{-2}$  and the initial temperature is larger than  $T \sim 10^4$  K, then the evolutionary path should hit this nearly vertical line (the long dashed line in Fig. 2). Because the line  $t_{\text{rec}} = t_{\text{cool}}$  is nearly vertical at  $T \simeq 10^4$  K and  $y_e \gtrsim 5 \times 10^{-2}$ ,  $y_e$  drops to several  $\times 10^{-2}$  without changing the temperature, and “forgets” the initial conditions, though  $y_e$  is not in chemical equilibrium. The value to which  $y_e$  converges ( $\sim 5 \times 10^{-2}$ ) is essentially determined by the equation  $t_{\text{rec}}(y_e, T) = t_{\text{cool}}^{\text{eq}}(y_e, T)$  at  $T \simeq 8000$  K. Here, the temperature 8000 K is obtained by the equality  $t_{\text{rec}}/t_{\text{cool}}^{Ly\alpha} = 1$ , where  $t_{\text{cool}}^{Ly\alpha}$  is the cooling time estimated by the hydrogen line cooling. The equation  $t_{\text{rec}}/t_{\text{cool}}^{Ly\alpha} = 1$  depends both on  $y_e$  and on  $T$  in general, but it depends only on  $T$  for  $y_e \ll 1$ .

The reason for the convergence of  $\text{H}_2$  also can be understood. According to Fig. 1,  $\text{H}_2$  is still in chemical equilibrium just below  $T = 10^4$  K, at which the convergence of  $y_e$  takes place. As a result, the systems that satisfy the previous condition (1) or (2) experience the same state (same  $y_e$ , same  $y_{\text{H}_2}$ ) just below  $T = 10^4$  K. Therefore  $y_{\text{H}_2}$  also converges for different initial conditions.

### 2.2.7. Comparizon with numerical calculations

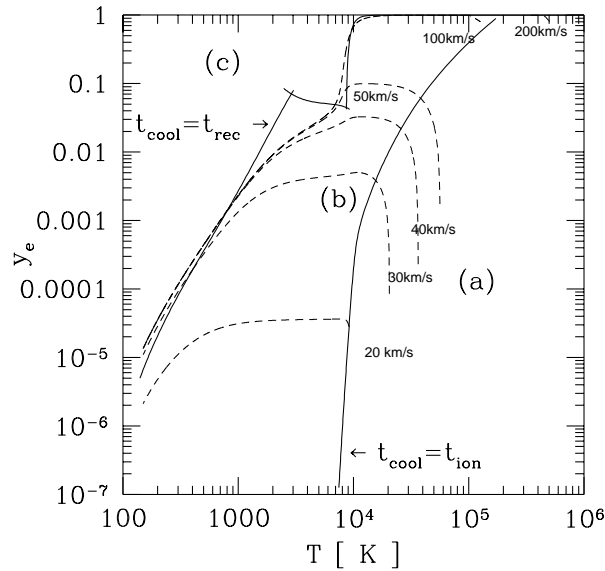


Fig. 3. The evolution of the post-shock layer in the  $y_e$ - $T$  plane. The solid lines are the boundaries beyond which the direction of evolution is changed, and each line has the same meaning as in Fig. 2. The short dashed lines are the numerical results. Each suffix denotes the initial shock velocity.

In this section we compare the results obtained in the previous section with numerical calculations. Figure 3 displays the evolution of  $y_e$  as a function of the temperature behind the shock front in steady flow. It is obvious that the expected evolutionary path in Fig. 2 agrees with the numerically calculated path. We also

find that there exists a critical value of the initial shock velocity above which the evolution of  $y_e$  below  $10^4$  K converges. The critical value of the shock velocity is  $\sim 40$  km/s. This condition for the initial shock velocity is equivalent to the condition (1) in the previous subsection.

Because of the delay of the recombination process compared to *the line cooling due to the hydrogen molecules*, fairly high degree of ionization ( $y_e \sim 10^{-1.5}$ ) is possible below 8000K. Fedded the electrons,  $H_2$  also maintains a high abundance ( $y_{H_2} \sim 10^{-2}$ ) for  $T \lesssim$  several  $\times 10^3$  K, then the cloud temperature drops to  $T \sim 100$  K quickly due to the  $H_2$  line cooling. In fact, the predicted evolutionary paths agree well with the numerically integrated paths for steady flow.

### 2.2.8. Fragmentation of the post-shock layer

To estimate the fragmentation condition of the post-shock layer, we can consider  $t_{\text{cool}}$  as  $t_{\text{dyn}}$  and  $t_{\text{ff}}$  as  $t_{\text{frag}}$ , where  $t_{\text{ff}}$  is the free-fall time scale, which corresponds to the growth time scale of gravitational instability.<sup>12)</sup> With the standard CDM cosmological model, we can estimate the fragmentation epoch.<sup>13), 14)</sup> As shown in Fig. 4,<sup>13)</sup> primordial gas clouds, which collapse in the early universe, fragment after they are cooled down to about 100 K if  $M \gtrsim 10^8 M_\odot$ . In the case that  $M \lesssim 10^8 M_\odot$ , the post-shock temperature is lower than  $10^4$  K, and  $H_2$  is formed only slightly. So, from the initial state in which  $t_{\text{cool}} > t_{\text{ff}}$ , the cloud evolves by gravitational force without cooling. Then the cloud will be virialized and cannot fragment, because it cannot be thin enough for fragmentation.

## §3. Collapse and fragmentation of filamentary clouds

A cooled sheet fragments more easily into filaments<sup>15), 16)</sup> than into spherical clouds. As the virial temperature of a filament is essentially *constant*, its evolution is much different from that of a spherical cloud, whose virial temperature increases as the cloud contracts. In this section, we investigate the evolution of filamentary clouds of primordial gas and estimate the fragmentation epoch.

### 3.1. Basic equations

We investigate the dynamical and thermal evolution with a 1-zone approximation for the simplicity.<sup>17)</sup> Then, basic equations are as follows. For an isothermal cylinder there is a critical line density  $M_c(T)$  given by

$$M_c(T) = \frac{2k_B T}{\mu m_H G}, \quad (3.1)$$

where  $T$ ,  $\mu$ , and  $m_H$  represent the isothermal temperature, the mean molecular weight and the mass of hydrogen atoms, respectively.<sup>18)</sup> An isothermal cylinder with line density  $M$  larger than  $M_c(T)$  has no equilibrium and collapses, while an isothermal cylinder with  $M$  less than  $M_c(T)$  expands if the external pressure does not exist.

When the filamentary cloud is formed as a result of the fragmentation of the sheet, the gas pressure is comparable to the gravitational force. Hence the effect of the gas pressure must be included in the equation of motion of the cylinder like cloud. To know the dynamical evolution of such a cylinder we begin with the virial

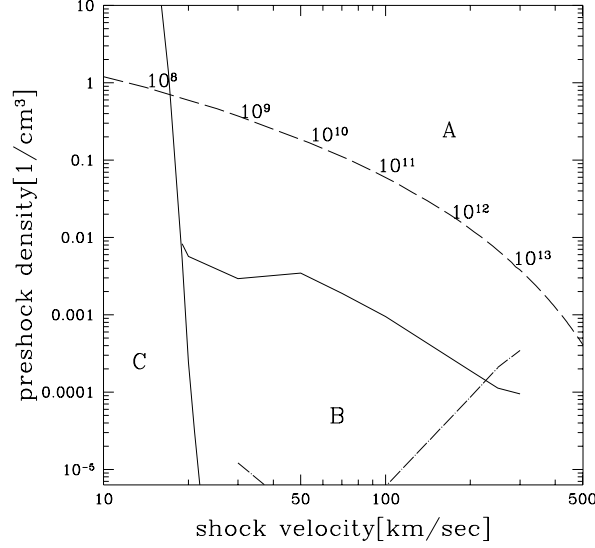


Fig. 4. Estimated fragmentation epoch. Pre-shock density-shock velocity plane, which is divided into three regions. Region *A* is where fragmentation occurs at low temperature  $\sim 100$  K, and region *B* is where it occurs at several thousand kelvin. In region *C* the post-shock temperature cannot rise above several thousand kelvin. Typical values of the shock velocity and the pre-shock density at the collapse in the standard CDM model are overplotted (dashed line). Numbers plotted above this line indicate the mass scales in unit of solar mass. The dot-dashed line divides the plane according to whether fragmentation occurs within 1 Gyr. The time elapsed since the point at which the shock front cross until fragmentation is calculated with  $z = 5$ . Most of the galactic sized clouds are cooled within 1 Gyr. Adapted from Yamada and Nishi (1998).

equation for a cylinder,

$$\frac{1}{2} \frac{d^2 I}{dt^2} = 2T + 2\Pi - GM^2, \quad (3.2)$$

where

$$I = \int_V \rho r^2 dV, \quad T = \int_V \frac{1}{2} \rho u^2 dV, \quad \Pi = \int_V p dV, \quad (3.3)$$

and the integration is effected over the volume per unit length of the cylinder,  $V$ . Here we assume that the cylinder is uniform and has constant density  $\rho$ , scale radius  $R = \sqrt{M/\pi\rho}$ , and temperature  $T$ . Then  $I$ ,  $T$  and  $\Pi$  introduced above become

$$I = \frac{1}{2} MR^2, \quad T = \frac{1}{4} M \left( \frac{dR}{dt} \right)^2, \quad \Pi = \frac{k_B T}{\mu m_H} M. \quad (3.4)$$

Substituting Eq. (3.4) in Eq. (3.2) we obtain

$$\frac{d^2 R}{dt^2} = -\frac{2G}{R} (M - M_c(T)). \quad (3.5)$$

We describe the evolution of the cylinder by this equation.

The time evolution of the cloud temperature is described by the energy equation given by

$$\frac{d\varepsilon}{dt} = -P \frac{d}{dt} \frac{1}{\rho} - \Lambda_{\text{rad}} - \Lambda_{\text{chem}}, \quad (3-6)$$

where  $\varepsilon$ ,  $\Lambda_{\text{rad}}$  and  $\Lambda_{\text{chem}}$  are the thermal energy per unit mass, the cooling by the radiation, and the cooling/heating by chemical reactions, respectively.

Assuming that the collapsing cylinder fragments when the condition (2-1) is satisfied, we estimate the epoch of fragmentation and the mass of fragments. The estimated mass scales correspond to the stellar mass scale ( $1M_{\odot} \sim 100M_{\odot}$ ).

### 3.2. Analytical estimate of the minimum fragment mass

Now, we estimate the minimum fragment mass analytically. As the cylinder collapses isothermally as a function of time in the later stage, we can set  $d\varepsilon/dt \sim 0$  in Eq. (3-6) and from this we obtain  $t_{\text{dyn}} \sim (\gamma - 1)t_{\text{cool}}$ , where  $\gamma = 7/5$  for a diatomic molecular gas. Since the cloud cools by the line emissions of hydrogen molecules and is optically thick to these line emissions,  $t_{\text{cool}}$  can be estimated by

$$t_{\text{cool}} \sim \frac{\frac{1}{\gamma-1} \frac{M}{\mu m_{\text{H}}} k_{\text{B}} T}{2\pi R \sigma T^4 \frac{\Delta\nu}{\nu} \alpha_c}, \quad (3-7)$$

where  $\sigma = 2\pi^5 k_{\text{B}}^4 / 15h^3 c^2$  is the Stefan-Boltzmann constant, and  $\alpha_c$  is the effective number of line emissions. Since the optical depth is  $\sim 100$  at most, the wing of the line profile may not be important,<sup>19)</sup> and the line broadening is determined by Doppler broadening as  $\Delta\nu/\nu = v_{\text{H}_2}/c = \sqrt{k_{\text{B}} T / m_{\text{H}} c^2}$ . The temperature of the cylinder is estimated by the virial temperature as

$$k_{\text{B}} T = \frac{1}{2} \mu m_{\text{H}} G M. \quad (3-8)$$

From the above equations we can estimate the fragment mass as

$$M_{\text{frag}} \sim 2\pi R M \sim \sqrt{\frac{1}{\alpha_c} \frac{1}{\mu^{9/4}} \frac{m_{\text{Pl}}^3}{m_{\text{H}}^2}}, \quad (3-9)$$

where  $m_{\text{Pl}} = \sqrt{\hbar c / G}$  is the Planck mass. Equation (3-9) implies that  $M_{\text{frag}}$  is essentially equal to the Chandrasekhar mass ( $\sim m_{\text{Pl}}^3 / m_{\text{p}}^2$ , where  $m_{\text{p}}$  is proton mass).

To this point we have not considered other heating processes, such as shocks and turbulence, which likely occur in a collapsing cloud. All these processes tend to halt the collapse, so that the epoch of fragmentation becomes earlier, and, as a result, the mass of fragments increases. Thus Eq. (3-9) gives a lower limit on the mass of the fragment which is formed from a primordial gas cloud. Our estimate shows that even a primordial gas cloud which cools most effectively by hydrogen molecules cannot fragment into a smaller mass than the expressed in Eq. (3-9).

For smaller line densities the gas pressure force halts the collapse before three-body reactions *completely* convert atomic hydrogen into molecules.<sup>6)</sup> In these cases, Eq. (3-9) is not applicable, because clouds are optically thin to line emissions if the

molecular fraction is smaller than about  $10^{-1}$ , and chemical heating by  $\text{H}_2$  formation must be considered when hydrogen molecules are formed by three-body reactions. These clouds fragment at lower density, in other words at larger scale radius. Since  $M_{\text{frag}}$  is proportional to the scale radius at fragmentation, this leads to the larger fragment mass.

In reality, numerical simulations suggest that primordial cylindrical clouds fragment at lower density, and the estimated masses of fragments are larger than the Chandrasekhar mass.<sup>16), 20)</sup>

#### §4. Evolution of cloud cores

Now we study the evolution process of cloud cores. After they collapse into stellar cores, true stars can form.

##### 4.1. Quasi-static contraction

The manner in which primordial clouds of stellar mass, which are fragments of filamentary clouds, evolve after the fragmentation depends on their efficiency of cooling, i.e., the ratio of the free-fall time scale  $t_{\text{ff}}$  to the cooling time scale  $t_{\text{cool}}$ . If  $t_{\text{ff}} < t_{\text{cool}}$  (i.e., cooling is not effective), while the cloud cools it has enough time to adjust itself to a new hydrostatic configuration. Then it contracts, maintaining a nearly hydrostatic equilibrium (i.e. Kelvin-Helmholtz contraction). On the other hand, in the case  $t_{\text{ff}} > t_{\text{cool}}$ , the cloud collapses dynamically in its free-fall time scale after substantial cooling, and no hydrostatic equilibrium is established.

At the time of the fragmentation of filamentary clouds, the two time scales of fragments,  $t_{\text{cool}}$  and  $t_{\text{ff}}$ , are of the same order of magnitude.<sup>17)</sup> Thus we investigate quasi-static contraction of cloud cores as a first step.<sup>21)</sup>

##### 4.1.1. Radiative processes in primordial molecular cloud cores

We consider spherically symmetric gas clouds with stellar mass ( $\sim 1M_{\odot}$ ) ('molecular cores') composed only of  $\text{H}_2$  molecules, because the hydrogen atoms are converted into molecular form before the fragmentation for these low mass fragments.<sup>17)</sup> We can neglect helium, since it is thermally inert at these low temperatures. As mentioned above, these clouds lose their thermal energy by radiative cooling via the  $\text{H}_2$  rotovibrational lines, and presumably contract into protostars.

In this section, we describe our calculation scheme for the luminosity and cooling rate of a spherically symmetric cloud. The specific intensity  $I_{\nu}$  ( $\text{ergs sec}^{-1} \text{cm}^{-2} \text{sr}^{-1} \text{Hz}^{-1}$ ) along a ray is calculated by solving the radiative transfer equation,<sup>19)</sup>

$$\frac{dI_{\nu}}{ds} = -\alpha_{\nu}I_{\nu} + j_{\nu}. \quad (4.1)$$

Here  $s$  is the displacement along the ray, and  $\alpha_{\nu}$  and  $j_{\nu}$  are the absorption and emission coefficients, respectively. These coefficients can be written using Einstein  $A$ - and  $B$ -coefficients:

$$j_{\nu} = \frac{h\nu}{4\pi}n_2A_{21}\phi(\nu), \quad (4.2)$$

$$\alpha_\nu = \frac{h\nu}{4\pi} \phi(\nu)(n_1 B_{12} - n_2 B_{21}). \quad (4.3)$$

Here  $n_1$  and  $n_2$  are the number densities of the molecules in the lower and upper levels of the transition, respectively, and  $\phi(\nu)$  is the line profile function. In our calculation, the line center optical depth of the lines across a cloud  $\tau_c$  is no more than about several hundred. Since the Lorentz wings of a line become more important than its Doppler core only when  $\tau_c$  is as large as  $10^3$ , we only consider line broadening owing to the thermal Doppler effect.

Note that the critical number density  $n_{\text{cr}}$ , where radiative and collisional de-excitation rates become equal for molecular hydrogen, is  $\sim 10^4 \text{ cm}^{-3}$ . Thus, for a typical number density of fragments ( $\sim 10^{10} \text{ cm}^{-3} \gg n_{\text{cr}}$ ), almost all excited molecules would be deexcited by collision with other molecules. Therefore, collisional local thermodynamic equilibrium (LTE) is established, and the scattering of photons can be neglected. These properties make the transfer problem of  $\text{H}_2$  lines fairly tractable.

#### 4.1.2. Evolution of fragments

As initial conditions, we assume polytropic gas spheres in hydrostatic equilibrium; namely the density/temperature distribution is represented by the Emden function of polytropic index  $N$ . Clouds are cut off at the radius  $r_s$ , where the density falls off by a factor of  $10^{-3}$  from the central value. Therefore, the parameters characterizing initial conditions are the effective polytropic index  $N$ , the total mass of the cloud  $M$ , and the number density  $n_h$  at the half mass radius. For a given initial configuration, we can obtain the specific entropy distribution  $s(m, t = 0)$ .

We calculate quasi-static contraction as follows. First we calculate the cooling rate  $\Lambda(m)$ , and advance the specific entropy distribution  $s(m, t)$  using the heat equation

$$\frac{\partial s}{\partial t} = -\frac{1}{T} \Lambda(m). \quad (4.4)$$

With the new entropy distribution, we find the new equilibrium configuration using the equations of hydrostatic equilibrium.

For given states of clouds, we compare two time scales, the free-fall time

$$t_{\text{ff}}(m) \equiv \sqrt{\frac{3\pi}{32G\bar{\rho}(m)}}, \quad (4.5)$$

and the time scale of quasi-static contraction,

$$t_{\text{qsc}}(m) \equiv \rho / \left( \frac{\partial \rho}{\partial t} \right)_{m, \text{quasi-static}}. \quad (4.6)$$

Here,  $\bar{\rho}(m)$  is the mean density at the mass coordinate  $m$ , and each quantity is evaluated at the coordinate  $m$ . From the virial theorem, we know that  $t_{\text{qsc}}$  is of the same order of magnitude as  $t_{\text{cool}}$ .

Figure 5 displays the contours of the ratio  $t_{\text{ff}}/t_{\text{qsc}}$  at the center ( $m = 0$ ) of clouds with (a)  $N = 2.5$  (adiabatic stratification) and (b)  $N = 8$ . Regions around

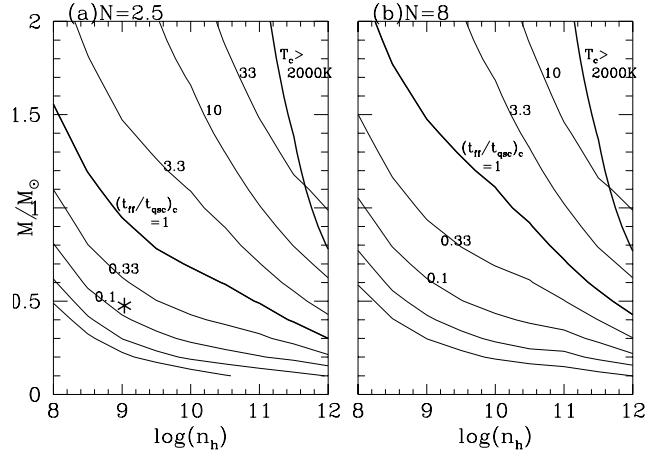


Fig. 5. Contours of the ratio  $t_{\text{ff}}/t_{\text{qsc}}$  at the centers of clouds of polytropic index (a)  $N = 2.5$  and (b)  $N = 8$ . The contour spacing is logarithmic with an increment of 0.5. The upper-right regions correspond to temperatures  $T > 2000$  K, where hydrogen molecules begin to dissociate. Adapted from Omukai et al. (1998)

the curves  $t_{\text{ff}}/t_{\text{qsc}} = 1$  are expected to be initial states of fragments. Although Fig. 5 displays the values at the center, this ratio does not change significantly within a cloud, except near the surface. The upper-right regions correspond to higher central temperature  $> 2000$  K, where the molecular hydrogen begins to dissociate. From the two panels of Fig. 5, we can see that the ratio  $t_{\text{ff}}/t_{\text{qsc}}$  depends only slightly on the effective polytropic indices  $N$ , rather than on masses and densities. Note that for clouds of the same mass, the ratio  $t_{\text{ff}}/t_{\text{qsc}}$  is greater for the denser cloud. This implies that as a cloud contracts, the ratio  $t_{\text{ff}}/t_{\text{qsc}}$  becomes larger. In particular, for fragments of filamentary gas clouds, for which  $t_{\text{ff}} \sim t_{\text{qsc}}$  initially,  $t_{\text{qsc}}$  becomes shorter than  $t_{\text{ff}}$  as they contract; i.e., such clouds collapse dynamically. Note that when  $t_{\text{qsc}} < t_{\text{ff}}$ , clouds do not contract quasi-statically, and  $t_{\text{qsc}}$  does not possess the meaning of the collapse time scale. In this case,  $t_{\text{qsc}}$  merely measures the time scale of cooling.

Figure 6 exhibits the change of time scales and their ratio for the quasi-static contraction of a cloud which is initially at the asterisk position of Fig. 5. We can see that the cloud indeed collapses dynamically after it contracts quasi-statically to some extent.

#### 4.1.3. Line profile and cooling rate

We have shown that the stellar mass molecular cores collapse dynamically, although some lines are optically thick at the line center. This fact indicates that the efficiency of cooling by  $\text{H}_2$  lines does not fall significantly even in such a situation, in contrast to the case of continuous radiation. The reason for this can be interpreted as follows.

Figure 7 displays the change of a processed profile of a single optically thick

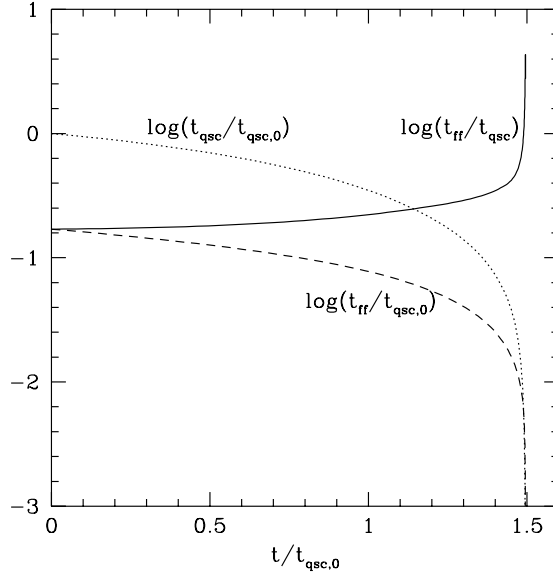


Fig. 6. Evolution of the free-fall time  $t_{\text{ff}}$  and dynamical time for quasi-static contraction  $t_{\text{qsc}}$  and their ratio at the center for a cloud which contracts quasi-statically at the beginning (asterisk of Fig. 5). The time scales  $t_{\text{ff}}$  and  $t_{\text{qsc}}$  and the time elapsed from the beginning  $t$  are all normalized by  $t_{\text{qsc},0}$ , the initial value of  $t_{\text{qsc}}$ . This figure indeed shows that the cloud begins to collapse dynamically after  $\sim 1.5 t_{\text{qsc},0}$ . Adapted from Omukai et al. (1998)

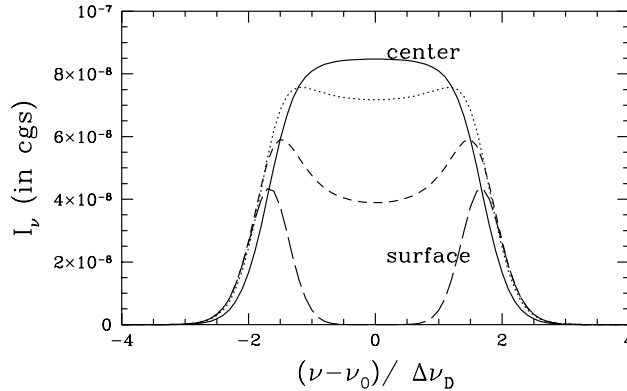


Fig. 7. Processed line profiles of an optically thick line along a ray passing through the center of a cloud at radii containing 0% (center, solid line), 1.4% (dotted line), 9.9% (short dashed line), and 100% (surface, long dashed line) of the total mass. The optical depth at the line-center frequency  $\tau_c = 38, 46, 54$  and  $76$ , respectively, measured from the surface of incidence. The line corresponds to the transition from  $(v = 1, j = 3)$  to  $(v = 0, j = 1)$ . The parameters of the cloud are the same as in Fig. 2. The abscissa represents the frequency from the line center normalized by the Doppler width at the center of the cloud  $\Delta\nu_{\text{D},c}$ . Adapted from Omukai et al. (1998)



line (optical depth at line center across the cloud is 76) along a ray passing through the center of the cloud. Since the cloud is optically thick at line center, the specific intensity at line center is saturated with the blackbody value determined from the local temperature. On the other hand, the optical depth at the wing is smaller than unity. The final processed profile at the cloud surface is double peaked, and the peak frequencies correspond to frequencies where the optical depth across the core  $\tau_{\nu,\text{core}} > 1$  (i.e., the radiation is saturated with the value of the core temperature) and that of envelope  $\tau_{\nu,\text{env}} < 1$  (i.e., the radiation can be larger than the value of the envelope temperature). The height (i.e., the normalization of intensity) and width of these peaks are of the same order of magnitude as the blackbody value determined from the temperature near the center, not around the surface of the cloud. The reduction factors from the central values are smaller than about 10. Owing to the effect described above, which is a distinctive feature of line cooling, the temperature around the cloud center can be ‘seen’ from outside the cloud, even when lines are optically thick at line center and the surface temperature is relatively low. Accordingly, its cooling proceeds efficiently, as long as there are enough frequency ranges where  $\tau_{\nu,\text{core}} > 1$  and  $\tau_{\nu,\text{env}} < 1$ . Therefore, the decrease in the efficiency of cooling caused by the low surface temperature is not severe in the line cooling case, in contrast to the case of cooling by continuum.

#### 4.2. Dynamical collapse of primordial protostellar clouds

As discussed above, although the cooling time of a cloud is longer than its free-fall time initially, the cooling time at the center becomes shorter than the free-fall time, and the cloud begins to dynamical collapse after some quasi-static contraction. In this section we investigate the dynamical collapse of primordial protostellar clouds and the formation of stellar cores.<sup>21)</sup>

##### 4.2.1. Method of calculation

We assume spherical symmetry for the simplicity. Then the Lagrangian equations describing dynamical collapse are as follows.

Equation of continuity:

$$\frac{\partial m}{\partial r} = 4\pi r^2 \rho, \quad (4.7)$$

equation of motion:

$$\frac{Dv}{Dt} = -4\pi r^2 \frac{\partial p}{\partial m} - \frac{Gm}{r^2}, \quad (4.8)$$

equation of energy:

$$\frac{D\epsilon}{Dt} = -p \frac{D}{Dt} \left( \frac{1}{\rho} \right) - \frac{\Lambda}{\rho}, \quad (4.9)$$

equation of state:

$$p = (\gamma_{ad} - 1)\rho\epsilon. \quad (4.10)$$

In the above expressions,  $m$ ,  $\rho$ ,  $v$ ,  $p$ ,  $\epsilon$ ,  $\Lambda$  and  $\gamma_{ad}$  are the mass within a radius  $r$ , the density, velocity, pressure, thermal energy per unit mass, net cooling rate per unit volume and the adiabatic coefficient, respectively.

The net cooling rate  $\Lambda$  consists of two parts, the radiative part  $\Lambda_{\text{rad}}$  and the chemical part  $\Lambda_{\text{chem}}$ .  $\Lambda_{\text{rad}}$  can be written as

$$\Lambda_{\text{rad}}(m) = \rho \frac{\partial L(m)}{\partial m}, \quad (4.11)$$

where  $L(m)$  is the luminosity and is obtained by solving radiative transfer equations. We consider  $\text{H}_2$  lines and continuum components which consist of  $\text{H}_2$  collision-induced absorption (CIA),  $\text{H}^-$  bound-free absorption, Lyman continuum absorption, etc. as sources of opacity.  $\Lambda_{\text{chem}}$  is given by

$$\Lambda_{\text{chem}}(m) = \rho \frac{\partial \epsilon_{\text{chem}}(m)}{\partial t}, \quad (4.12)$$

where  $\epsilon_{\text{chem}}$  is the chemical binding energy per unit mass.

#### 4.2.2. Dynamical evolution of protostellar clouds

The evolutionary sequences of the radial profiles of number density, temperature, velocity and  $\text{H}_2$  concentration distributions are illustrated in Fig. 8.

The collapse proceeds almost self-similarly and is analogous to the Larson-Penston similarity solution<sup>23)</sup> until the central region reaches the stellar density. The dashed line in the figure indicates the slope of density gradient of  $-2$ . The slope in this case is slightly steeper and its value is about  $-2.2$ , which correspond to the effective adiabatic index is 1.1.

At higher density, almost all hydrogens are converted to  $\text{H}_2$  by efficient three-body processes. But the total mass of central molecular part is about  $1 M_{\odot}$  which hardly depends on total cloud mass. When the central number density reaches about  $3 \times 10^{13} \text{ cm}^{-3}$  and the central temperature reaches about 1600 K, the hydrogen molecules begin to dissociate gradually. But at almost the same time,  $\text{H}_2$  CIA continuum cooling becomes efficient. This continuum cooling is so strong to stop and even to reverse dissociation. After a small central part of the cloud becomes opaque to CIA continuum ( $3 \times 10^{16} \text{ cm}^{-3}$ , 2000 K), the effective dissociation begins.

The evolution of the temperature and the effective ‘adiabatic index’  $\Gamma = \frac{\partial \ln p / \partial t}{\partial \ln \rho / \partial t}$  at the center for various total mass cases are illustrated in Fig. 9. We can see the central value  $\Gamma$  is about 1.1 almost throughout the collapse. After some contraction, evolution paths of the central regions are hardly affected by the total mass.

When most of the  $\text{H}_2$  molecules are dissociated,  $\Gamma$  rises above the critical value  $4/3$ . After the central part of the cloud contracts almost adiabatically to some extent, a hydrostatic core with very small mass ( $\sim 5 \times 10^{-3} M_{\odot}$ ) forms at the center. At that time, the central number density and temperature are  $\sim 10^{22} \text{ cm}^{-3}$  and  $\sim 3 \times 10^4 \text{ K}$ . These values are almost the same as those of present-day stellar cores at the formation epoch.

But before the formation of the stellar core, no transit core is formed, in contrast to the case of present-day star formation. And the estimated mass accretion rate in the case of primordial star formation is much different from that of present-day star formation ( $\sim 10^{-5} M_{\odot} \text{ yr}^{-1}$ ), as shown below. Before stellar core formation, the radial profiles of the density are well fitted by the Larson-Penston-type similarity

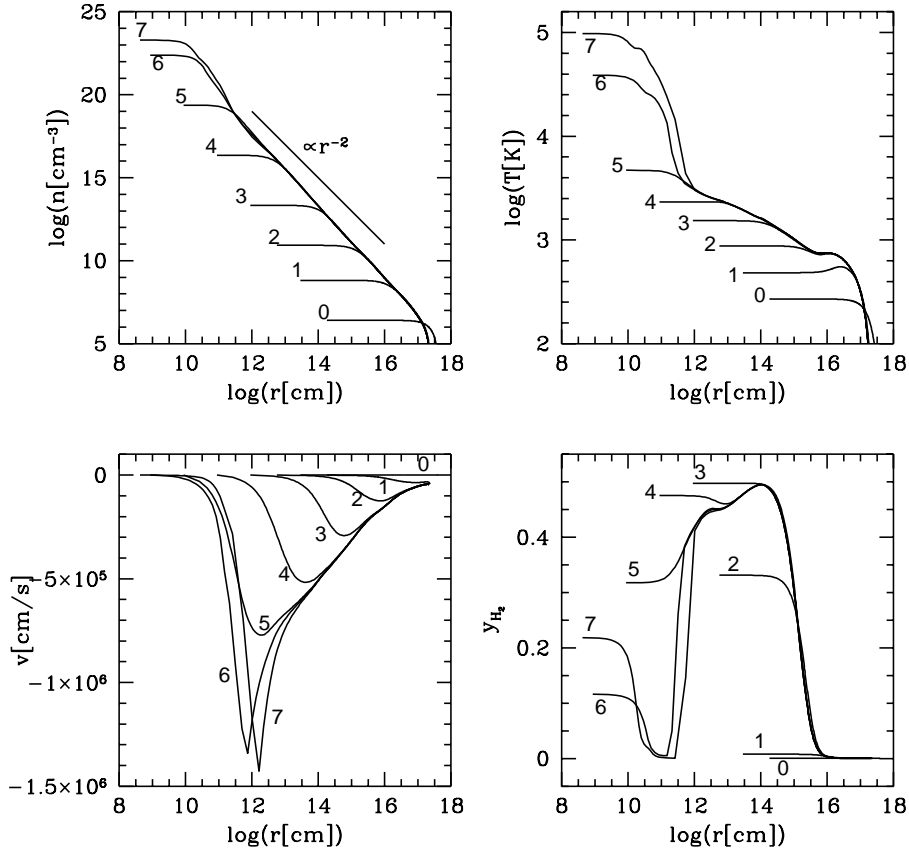


Fig. 8. The radial profiles of the physical quantities. (a) The number density ( $n \equiv \rho/m_{\text{H}}$ , where  $m_{\text{H}}$  is the mass of the hydrogen atom), (b) temperature, (c) velocity, and (d) the  $\text{H}_2$  concentration are given as functions of the radial distance. The numbers in the figure denote the evolutionary sequences. ‘0’ corresponds to the initial time, and ‘1’ to  $5.7 \times 10^5$  yrs after starting calculation. Here, three-body processes are active in the central region and temperature inversion occurs because of efficient  $\text{H}_2$  line cooling. ‘2’ corresponds to  $8.5 \times 10^3$  yrs after state 1: The cloud becomes optically thick to some  $\text{H}_2$  lines. ‘3’ corresponds to  $2.8 \times 10^2$  yrs after state 2: The central region becomes fully molecular. ‘4’ corresponds to 12 yrs after state 3: The central region become optically thick to the  $\text{H}_2$  CIA continuum. ‘5’ corresponds to 0.32 yrs after state 4:  $\text{H}_2$  dissociation becomes efficient. ‘6’ corresponds to  $2.4 \times 10^{-2}$  yrs after state 5: Shortly after the core formation. ‘7’ corresponds to  $4.1 \times 10^{-2}$  yrs after state 6. Adapted from Omukai and Nishi (1998)

solution with  $\gamma = 1.09$ . Assuming that the evolution of an envelope after stellar core formation is described by the same similarity solution, we can estimate the evolution of the core mass. With the similarity solution after the central density becoming infinite, we have for the central stellar mass<sup>24)</sup>

$$M_* = 0.11M_{\odot} \left( \frac{t}{1 \text{ yr}} \right), \quad (4.13)$$

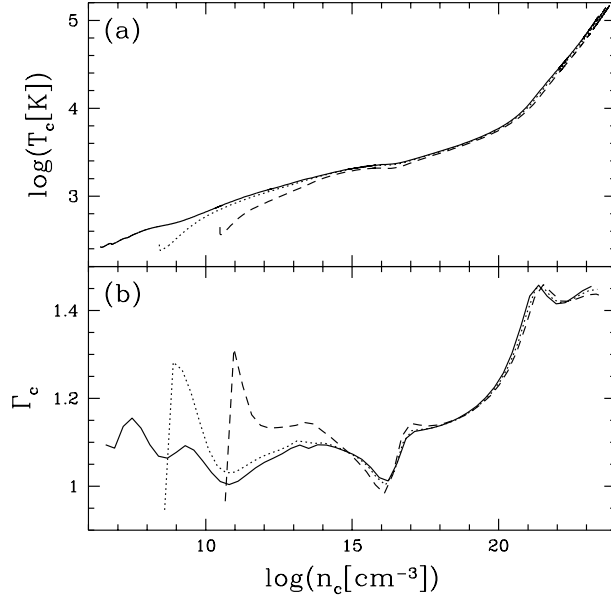


Fig. 9. The temperature and effective ‘adiabatic index’  $\Gamma$  at the central regions are plotted against the central number density  $n_c$  [ $\text{cm}^{-3}$ ] for clouds with various masses. (a) The central temperature  $T_c$ . (b) The effective ‘adiabatic index’  $\Gamma_c$  in the central regions. In both panels, the total masses are  $10^2 M_\odot$  (solid lines),  $10 M_\odot$  (dotted lines) and  $1 M_\odot$  (dashed lines). Adapted from Omukai and Nishi (1998)

and we can estimate the mass accretion rate as

$$\dot{M}_* = 8.3 \times 10^{-2} M_\odot \text{ yr}^{-1} \left( \frac{t}{1 \text{ yr}} \right)^{-0.27}, \quad (4.14)$$

$$= 3.7 \times 10^{-2} M_\odot \text{ yr}^{-1} \left( \frac{M_*}{M_\odot} \right)^{-0.37}. \quad (4.15)$$

The mass accretion rate is very large and diminishes with time. The main reason for this large mass accretion rate is that the temperature of primordial gas clouds ( $\sim 10^3$  K) is higher (which is the result of weak cooling) than that of the present-day molecular clouds ( $\sim 10$  K). The final stellar mass may be large because of the large mass accretion rate.

## §5. Summary and discussion

We investigated the thermal and the dynamical evolution of primordial gas clouds in the universe after decoupling and discussed the fragmentation process. It is necessary to study the evolution of the clouds considering the change of cloud shapes. Comparing the time scale of the dynamical evolution with that of fragmentation, we estimated the typical fragmentation scale.

## 5.1. A formation scenario of first luminous objects

We propose a formation scenario for first luminous objects (Fig. 10):

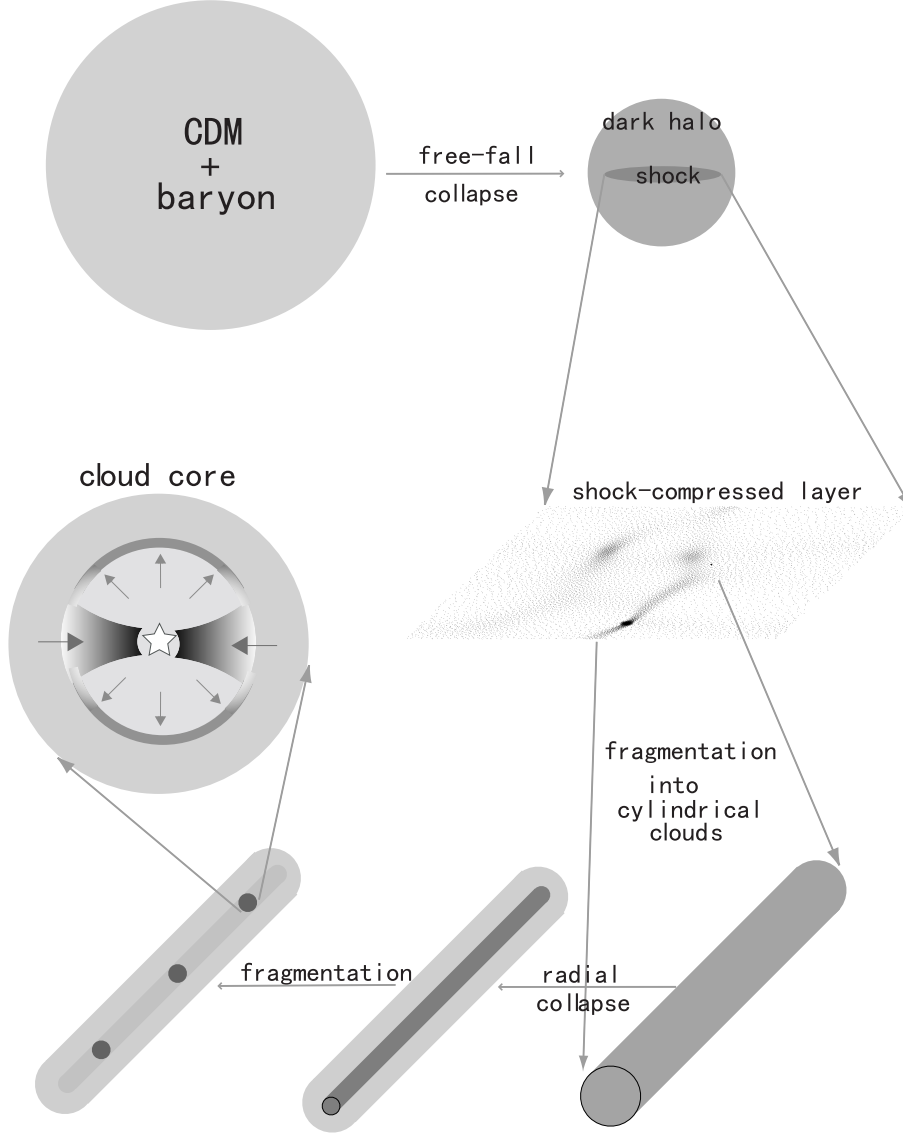


Fig. 10. The formation scenario for first luminous objects.

- (1) By pancake collapse of the over-density regions or collision between clouds in potential wells, quasi-plane shocks form.
- (2) If the shock-heated temperature is higher than about  $10^4$  K, the post-shock gas cools by  $H_2$  line cooling, and the shock-compressed layer fragments into cylindrical clouds when  $t_{\text{dyn}} \sim t_{\text{frag}}$  ( $T$  is several hundred K).
- (3) The cylindrical cloud collapses dynamically once more and fragments into cloud cores when  $t_{\text{dyn}} \sim t_{\text{frag}}$ .

- (4) A primordial star forms in a cloud core.
- (5) In the case that the shock-heated temperature is higher than about  $10^4$  K, many fragments can be formed almost simultaneously. Thus, many massive stars may be formed within the time scale of the life of massive stars.
- (6) Luminous objects are formed.

The condition (5) is achieved when a massive cloud ( $\gtrsim 10^8 M_\odot$ ) collapses or subgalactic clouds collide with each other in the potential of massive objects, which has the virial velocity larger than about 40 km/s. In any case, luminous objects can be formed after massive objects ( $M \gtrsim 10^8 M_\odot$ ) collapse.

In the case that the shock-heated temperature is lower than about  $10^4$  K, ionization can not occur and  $H_2$  molecules are formed only with cosmological relic electrons. Hence  $y_{H_2}$  is small and cooling by  $H_2$  is weak, and the cloud cannot fragment into many small clouds. In this case, one or a few massive stars may be formed around the cloud center. After the first generation of massive stars are formed, the cooling of the remaining part of the cloud becomes inefficient, since hydrogen molecules are dissociated by UV photons radiated by massive stars. Thus, the star formation rate is strongly self-regulated.<sup>25)</sup> Moreover, the binding energy of such a small mass cloud is small, and the cloud is blown off or disturbed severely by a super nova explosion, and as a result, the formation of the next generation of stars is greatly delayed. Then it is unlikely for isolated small mass clouds to become luminous objects.

### Acknowledgements

We thank H. Sato and T. Nakamura continuous encouragement. This work is supported in part by Research Fellowships of the Japan Society for the Promotion of Science for Young Scientists, No. 2370 (HS), 6894 (HU) and Grant-in-Aid for Scientific Research on Priority Areas (No. 10147105) (RN) and Grant-in-Aid for Scientific Research from the Ministry of Education, Science, Sports, and Culture, No. 08740170 (RN).

### References

- [1] M. Fukugita and M. Kawasaki, *Mon. Not. R. Astron. Soc.* **269** (1994), 563.  
J. P. Ostriker and N. Y. Gnedin, *Astrophys. J.* **472** (1996), L63.  
Z. Haiman and A. Loeb, *Astrophys. J.* **483** (1997), 21.
- [2] D. Galli and F. Palla, *Astron. Astrophys.* **335** (1998), 403.
- [3] T. Matsuda, H. Sato and H. Takeda, *Prog. Theor. Phys.* **42** (1969), 219.
- [4] J. B. Hutchins, *Astrophys. J.* **205** (1976), 103.
- [5] R. G. Carlberg, *Mon. Not. R. Astron. Soc.* **197** (1981), 1021.
- [6] F. Palla, E. E. Salpeter and S. W. Stahler, *Astrophys. J.* **271** (1983), 632.
- [7] C. C. Lin, L. Mestel and F. H. Shu, *Astrophys. J.* **142** (1965), 1431.
- [8] H. Susa, H. Uehara and R. Nishi, *Prog. Theor. Phys.* **96** (1996), 1073.
- [9] H. Susa, H. Uehara, R. Nishi and M. Yamada, *Prog. Theor. Phys.* **100** (1998), 63.
- [10] P. R. Shapiro and H. Kang, *Astrophys. J.* **318** (1987), 32.
- [11] H. Uehara and R. Nishi, in preparation.
- [12] B. G. Elmegreen and D. M. Elmegreen, *Astrophys. J.* **220** (1978), 1051.
- [13] M. Yamada and R. Nishi, *Astrophys. J.*, **505** (1998), 148.
- [14] H. Uehara and R. Nishi, *Astrophys. J.*, (1998), accepted.
- [15] S. M. Miyama, S. Narita, and C. Hayashi, *Prog. Theor. Phys.* **78** (1987), 1051, 1273.

- [16] H. Uehara, Ph. D Thesis, Kyoto University (1998).
- [17] H. Uehara, H. Susa, R. Nishi, M. Yamada and T. Nakamura, *Astrophys. J. Lett.* **473** (1996), L95.
- [18] J. Ostriker, *Astrophys. J.* **140** (1964), 1056.
- [19] G. B. Rybicki and A. P. Lightman, *Radiative Process in Astrophysics* (Wiley-Interscience, New York, 1979).
- [20] F. Nakamura and M. Umemura, *Proc. IAU Sympo. 187 Cosmic Chemical Evolution* (1998).
- [21] K. Omukai, R. Nishi, H. Uehara and H. Susa, *Prog. Theor. Phys.* **99** (1998), 747.
- [22] K. Omukai and R. Nishi, *Astrophys. J.* (1998), in press.
- [23] R. B. Larson, *Mon. Not. R. Astron. Soc.* **145** (1969), 271.  
M. V. Penston, *Mon. Not. R. Astron. Soc.* **144** (1969), 425.
- [24] A. Yahil, *Astrophys. J.* **265** (1983), 1047.  
Y. Suto and J. Silk, *Astrophys. J.* **326** (1988), 527
- [25] K. Omukai and R. Nishi, *Astrophys. J. Lett.* (1998), accepted.